Journal of Heat and Mass Transfer Research

Journal homepage: https://jhmtr.semnan.ac.ir

Semnan University

ISSN: 2383-3068

Research Article

Analysis of MHD Thermosolutal Convection in a Porous Cylindrical Cavity Filled with a Casson Nanofluid, Considering Soret and Dufour Effects

Mustapha El Hamma [a]*, Ilham Aberdane [a], Mohammed Taibi [a,b], Ahmed Rtibi [a], Kamal Gueraoui [a]

[a] *Department of Physics, Team of Modeling and Simulation in Mechanics and Energetics (MSME), Faculty of Sciences, Mohammed V University in Rabat, Morocco.*

[b] *Labo of Mechanics, University of Hassan II of Casablanca, Faculty of Sciences, Morocco.*

ARTICLE INFO

Article history:

Received: 2023-05-02

Revised: 2023-11-02

Accepted: 2023-11-04

Keywords:

Casson nanofluid;

Extension of the Law of Darcy;

MHD thermosolutal convection;

Soret and dufour effects.

ABSTRACT

The aim of this work is to numerically and theoretically model thermosolute natural convection in porous, isotropic and saturated media filled with Casson nanofluids (aluminum nanoparticles) under the influence of a magnetic field. Calculations were performed for various parameters relevant to our model, namely Casson fluid parameters (between 0.1 and 1), thermal Rayleigh number (between 10 and 100000), Geometric aspect ratio number (between 1 and 3),Buoyancy ratio number (between 1 and 10), Soret and Dufour numbers (between 0.2 and 1.2), conductivity ratios (between 1 and 3) and Hartmann numbers (between 0 and 100). The horizontal walls of the enclosure maintain uniform temperature and concentration, while the side walls are rigid, watertight, and insulated. Casson nanofluid flow occurs in porous layers and is described by the extended Darcy law of Brinkman-Forchheimer. The finite volume method was used to spatially discretize the obtained system of equations. Therefore, we investigated the effect of different parameters on the heat transfer rate and concentration. we observe that heat and mass transfer increases with increasing Casson fluid parameter; this increase is significant for the case of β between 0.1 and 0.4. And it also increases with the increase in the number of thermal conductivity ratios, the number of thrust ratios and with the increase in the thermal Rayleigh number. The latter remain unchanged when the thermal Rayleigh number is below the threshold $R_{T,nf} = 5 \times 10^2$. In the Opposite, we notice an uneven decrease in the thermosolutal transfer with the increase in the Hartmann Soret and Dufour numbers.

1. Introduction

The study of the phenomenon of heat and mass transfer is crucial for many fields of science and engineering; it allows to solve complex problems and to develop more efficient and more sustainable technologies, such as metallurgy, electrochemistry, biology, geophysics, chemical systems and processes. [1-4]. To this end, scientific researchers are much more interested in research on modeling the phenomenon of double diffusion convection in porous media. The work carried out on modelling the phenomenon of double diffusion convection in porous media is

* **Corresponding author.**
E-mail address: *mustapha_elhamma@um5.ac.ma*

Cite this article as:
El Hamma, M., Aberdane, I., Taibi, M., Rtibi, A., Gueraoui, K. 2023. Analysis of MHD Thermosolutal Convection in a Porous Cylindrical Cavity Filled with a Casson Nanofluid, Considering Soret and Dufour Effects, *Journal of Heat and Mass Transfer Research*, 10(2), pp. 197-206.

https://doi.org/10.22075/JHMTR.2023.30532.1439

diverse and focuses on the understanding of the fundamental mechanisms of heat and mass transfer, such as:

Hirpho et al. [5] were interested in the modeling and simulation of mixed convection of hybrid Casson nanofluids in a partially heated trapezoidal chamber.Shah et al. [6] investigated thermosolutal convection energy transfer in a magnetically influenced Casson fluid flow in a hexagonal enclosure with nets. Alwawi et al. [7] performed a study of the MHD natural convection of sodium alginate Casson nanoliquid in a solid sphere. Gbadeyan et al. [8] examined the effect of varying thermal conductivity and viscosity on the flow of Casson's nanofluid with convective heating. Haq et al. [9] studied the phenomenon of heat transfer by convection of a Casson nanofluid on a shrinkable sheet. Ibrahim et al. [10] studied the flow of three-dimensional MHD mixed convection of Casson nanofluid Hall effect and ion slip. Ganesh Kumar et al. [11] investigated the impact of convective condition on Marangoni convection flux and heat transfer in Casson nanofluid with uniform heat source sink.

Nadeem et al. [12] carried out a three-dimensional flow study of the MHD boundary layer of the Casson nanofluid in front of a linear stretch sheet with convective boundary conditions. Imtiaz et al. [13] studied the mixed convection flux of the Casson nanofluid on a stretching cylinder with convective boundary conditions. M.I. Khan et al. [14] carried out a modeling and numerical simulation of hybrid nanofluid flow ($SiO2/C3H8O2$) and ($MoS2/C3H8O2$) with optimization of entropy and variable viscosity. Alsabéry et al. [15] carried out a numerical study based on the finite difference method. This study emphasized; on the effect of the variable sinusoidal temperature through two lateral and opposite walls; on the natural convection flow of a nanofluid in a tilted square enclosure with a partially saturated porous layer. S. A. Khan et al. [16] studied the Melting heat transportation in radiative flow of nanomaterials with irreversibility analysis. Sheremet et al. [17] studied double diffusion mixed convection in an open porous space. The cavity is filled with a nanofluid (the basic nanofluid is a binary fluid such as salt water) and nanoparticles.

The influence of Reynold number, Lewis number and Rayleigh number has been studied. T. Hayat et al. [18] studied heat transportation in electro-magnetohydrodynamic flow of Darcy-Forchheimer viscous fluid with irreversibility analysis. Miroshnichenko et al. [19] studied MHD natural convection in a partially open trapezoidal cavity filled with a nanofluid. S. A. Khan et al. [20] were interested in Simultaneous features of Soret and Dufour in entropy optimized flow of reiner-rivlin fluid considering thermal radiation. Basak and al [21] carried out a study of natural convection in porous trapezoidal enclosures. The bottom wall is uniformly or unevenly heated. R.R. Kairi et al. [22] studied Stratified thermosolutal Marangoni bioconvective flow of gyrotactic microorganisms in Williamson nanofluid. R.R. Kairi et al. [23] carried out a Thermosolutal Marangoni Impact on Bioconvection in Suspension of Gyrotactic Microorganisms over an Inclined Stretching Sheet. M.Bernatchou et al. [24] performed a study of the Magnetic Field Effect on Thermosolutal Convection Heat and Mass Transfer in a Square Cavity Filled with Nanofluid. V. M. Magagula et al. [25] studied the Double dispersed bioconvective Casson nanofluid fluid flow over a nonlinear convective stretching sheet in suspension of gyrotactic microorganism.

S. Bilal et al. [26] carried out a Entropy analysis in a single phase nanofluid in square enclosure under effectiveness of inclined magnetic field by executing finite element simulations. I. A. Shah et al. [27] investigated the Convective Heat and Mass Transport in Casson Fluid Flow in Curved Corrugated Cavity with Inclined Magnetic Field. S. Bila et al. [28] were interested in Heat Transfer Enhancement of MHD Natural Convection in a Star-Shaped Enclosure, Using Heated Baffle and MWCNT–Water Nanofluid. A. Z. Ghadi et al. [29] were interested in Numerical modelling of double-diffusive natural convection within an arcshaped enclosure filled with a porous medium. A. I. Lare [30] studied the Casson Fluid Flow with Variable Viscosity and Thermal Conductivity along Exponentially Stretching Sheet Embedded in a Thermally Stratified Medium with Exponentially Heat Generation. O. Ghaffarpasand [31] were interested in Characterization of unsteady double-diffusive mixed convection flow with soret and dufour effects in a square enclosure with top moving lid.

The novelty of this work, compared to work [2] and [4,] is that it studies the modeling of thermosolutal convection in a porous, isotropic and saturated medium filled with a Casson nanofluid (binary basic fluid) under the effect of the thermo-diffusion phenomenon (Soret and Dufour effect) taking into account the effect of a magnetic field in the vertical direction. So, this work provides a study of convection with all the influences and the degree of their influence on convection thermosolutal . Among these effects that were studied in this work are the effect of the Casson parameter, Soret and Dufour effect, effect of the magnetic field, and effect of thermal conductivity on thermosolutal convection.

2. Mathematical Modeling of the Problem Studied

2.1. Flow Geometry

Thermosolute convection phenomena are investigated in cylindrical chambers filled with isotropic porous media and saturated with Casson nanofluids. The case in question (Fig. 1) consists of lower and upper bases, each exposed to uniform temperature and concentration. The side walls are assumed to be insulating and impermeabl.

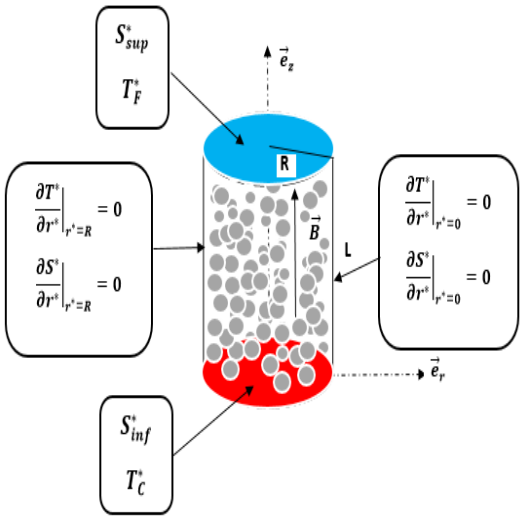

Fig. 1. Geometry of the studied problem

2.2. Governing Equations

The mathematical model reflecting the phenomenon studied is based on the conservation equations of continuum mechanics. Thus, the laws of Darcy-Brinkman-Forchheimer describe the flow of the nanofluid in the porous layers. The thermo-physical properties of the nanofluid are assumed constant. Governing equations are modeled and designed based on research [2]and[4].

Continuity equation

The continuity equation in dimensional form is written :

In vector form

$$\vec{\nabla}.\vec{V}^* = 0 \tag{1}$$

In scalar form

$$\frac{1}{r^*}\frac{\partial(r^*u^*)}{\partial r^*} + \frac{\partial w^*}{\partial z^*} = 0 \tag{2}$$

Conservation of Momentum Equation

The momentum conservation equation in dimensional form is written as:

In vector form

$$\left(\frac{1}{\varepsilon^2}(\vec{V}^*.\vec{\nabla})\vec{V}^*\right) = -\frac{\mu_{nf}}{\rho_{0nf}K}\vec{V}^* + \frac{\rho_{nf}}{\rho_{0nf}}\vec{g} - \frac{1}{\rho_{0nf}}\vec{\nabla}P + \frac{\widetilde{\mu_{nf}}}{\rho_{0nf}}\left(1+\frac{1}{\beta}\right)\Delta\vec{V}^* - \frac{C_F}{K^{\frac{1}{2}}}|\vec{V}^*|\vec{V}^* + \frac{1}{\rho_{0nf}}(\vec{J}\wedge\vec{B}) \tag{3}$$

with

$$\vec{J} = \sigma_{nf}\left(\vec{E} + (\vec{V}\wedge\vec{B})\right) \tag{4}$$

We apply the rotational operator to the equation (3), to obtain equation (5) in the scalar form

$$\begin{aligned}&\frac{1}{\varepsilon^2}\left(\frac{1}{r^*}\frac{\partial(r^*u^*\Omega^*)}{\partial r^*} + \frac{\partial(w^*\Omega^*)}{\partial z^*} - \frac{u^*\Omega^*}{r^*}\right)\\ &= -\frac{\mu_{nf}}{K\rho_{0nf}}\Omega^* - \frac{\rho_0(1-\varphi)}{\rho_{0nf}}\beta_T\, g\frac{\partial T^*}{\partial r^*}\\ &-\frac{\rho_0(1-\varphi)}{\rho_{0nf}}\beta_s\, g\frac{\partial S^*}{\partial r^*}\\ &+\frac{\widetilde{\mu_{nf}}}{\rho_{0nf}}\left(1+\frac{1}{\beta}\right)\left(\frac{\partial^2\Omega^*}{\partial r^{*2}} + \frac{1}{r^*}\frac{\partial\Omega^*}{\partial r^*} + \frac{\partial^2\Omega^*}{\partial z^{*2}} - \frac{\Omega^*}{r^{*2}}\right)\\ &-\frac{C_F}{K^{\frac{1}{2}}}|\vec{V}^*|\,\Omega^* + \frac{C_F}{K^{\frac{1}{2}}}\left(w^*\frac{\partial|\vec{V}^*|}{\partial r^*} - u^*\frac{\partial|\vec{V}^*|}{\partial z^*}\right)\\ &-\frac{1}{\rho_{0nf}}\sigma_{nf}B^2\frac{\partial u^*}{\partial z^*}\end{aligned} \tag{5}$$

Energy conservation equation

The energy conservation equation in dimensional form is written as:

In vector form

$$\vec{\nabla}.(\vec{V}^*T^*) = \alpha\Delta T^* + \varepsilon\, N_{TC}\Delta S^* \tag{6}$$

In scalar form

$$\begin{aligned}&\left(\frac{\partial(u^*T^*)}{\partial r^*} + \frac{\partial(w^*T^*)}{\partial z^*} + \frac{u^*T^*}{r^*}\right)\\ &= \alpha\left(\frac{\partial^2T^*}{\partial r^{*2}} + \frac{\partial^2T^*}{\partial z^{*2}} + \frac{1}{r^*}\frac{\partial T^*}{\partial r^*}\right)\\ &+\varepsilon\, N_{TC}\left(\frac{\partial^2S^*}{\partial r^{*2}} + \frac{\partial^2S^*}{\partial z^{*2}} + \frac{1}{r^*}\frac{\partial S^*}{\partial r^*}\right)\end{aligned} \tag{7}$$

Conservation of mass equation

The mass conservation equation in dimensional form is written:

In vector form

$$\vec{\nabla}.(\vec{V}^*S^*) = D\,\varepsilon\,\Delta S^* + \varepsilon\, N_{CT}\,\Delta T^* \tag{8}$$

In scalar form

$$\begin{aligned}&\left(\frac{\partial(u^*S^*)}{\partial r^*} + \frac{\partial(w^*S^*)}{\partial z^*} + \frac{u^*S^*}{r^*}\right)\\ &= D\,\varepsilon\left(\frac{\partial^2S^*}{\partial r^{*2}} + \frac{\partial^2S^*}{\partial z^{*2}} + \frac{1}{r^*}\frac{\partial S^*}{\partial r^*}\right)\\ &+\varepsilon\, N_{CT}\left(\frac{\partial^2T^*}{\partial r^{*2}} + \frac{\partial^2T^*}{\partial z^{*2}} + \frac{1}{r^*}\frac{\partial T^*}{\partial r^*}\right)\end{aligned} \tag{9}$$

The current function equation

The current function equation in dimensional form is written:

$$u^* = \frac{1}{r^*}\frac{\partial \psi^*}{\partial z^*} \tag{10}$$

$$w^* = -\frac{1}{r^*}\frac{\partial \psi^*}{\partial r^*} \tag{11}$$

$$\Omega^* = \frac{1}{r^*}\left(\Delta\psi^* - \frac{2}{r^*}\frac{\partial \psi^*}{\partial z^*}\right) \tag{12}$$

Dimensionless equations

The previously established equations are written in dimensionless form:

$$\frac{1}{r}\frac{\partial (ru)}{\partial r} + \frac{\partial w}{\partial z} = 0 \tag{13}$$

$$\begin{aligned}&\frac{1}{\varepsilon^{\,2}}\left(\frac{1}{r}\frac{\partial (rU\Omega)}{\partial r} + \frac{\partial (W\Omega)}{\partial z} - \frac{U\Omega}{r}\right)\\ &= -\bar{\Lambda}\frac{Pr_{nf}}{Da}\Omega - \bar{\Lambda}^2 R_{T,nf}\, Pr_{nf}\left(\frac{\partial \theta}{\partial r} + N\frac{\partial S}{\partial r}\right)\\ &+ \frac{\bar{\Lambda}\, Pr_{nf}}{\varepsilon}\left(1+\frac{1}{\beta}\right)\left(\frac{\partial^2 \Omega}{\partial r^2} + \frac{1}{r}\frac{\partial \Omega}{\partial r} + \frac{\partial^2 \Omega}{\partial z^2} - \frac{\Omega}{r^2}\right)\\ &- \frac{C_F}{\sqrt{Da}}\,|\vec{V}|\Omega + \frac{C_F}{\sqrt{Da}}\left(W\frac{\partial |\vec{V}|}{\partial \bar{r}} - U\frac{\partial |\vec{V}|}{\partial \bar{z}}\right)\\ &-\bar{\Lambda} Pr_{nf} Ha^2 \frac{\partial U}{\partial Z}\end{aligned} \tag{14}$$

$$\begin{aligned}&\frac{\partial (\mathrm{U}\theta)}{\partial \mathrm{r}} + \frac{\partial (\mathrm{W}\theta)}{\partial \mathrm{z}} + \frac{\mathrm{U}\theta}{\mathrm{r}}\\ &= \frac{\partial^2 \theta}{\partial \mathrm{r}^2} + \frac{\partial^2 \theta}{\partial \mathrm{z}^2} + \frac{1}{\mathrm{r}}\frac{\partial \theta}{\partial \mathrm{r}} + \varepsilon\,\mathrm{Du}\left(\frac{\partial^2 \mathrm{S}}{\partial \mathrm{r}^2} + \frac{\partial^2 \mathrm{S}}{\partial \mathrm{z}^2} + \frac{1}{\mathrm{r}}\frac{\partial \mathrm{S}}{\partial \mathrm{r}}\right)\end{aligned} \tag{15}$$

$$\begin{aligned}&\frac{\partial (\mathrm{US})}{\partial \mathrm{r}} + \frac{\partial (\mathrm{WS})}{\partial \mathrm{z}} + \frac{\mathrm{US}}{\mathrm{r}}\\ &= \frac{\varepsilon}{\mathrm{Le}}\left(\frac{\partial^2 \mathrm{S}}{\partial \mathrm{r}^2} + \frac{\partial^2 \mathrm{S}}{\partial \mathrm{z}^2} + \frac{1}{\mathrm{r}}\frac{\partial \mathrm{S}}{\partial \mathrm{r}}\right)\\ &+ \frac{\varepsilon}{\mathrm{Le}}\mathrm{Sr}\left(\frac{\partial^2 \theta}{\partial \mathrm{r}^2} + \frac{\partial^2 \theta}{\partial \mathrm{z}^2} + \frac{1}{\mathrm{r}}\frac{\partial \theta}{\partial \mathrm{r}}\right)\end{aligned} \tag{16}$$

$$U = \frac{1}{r}\frac{\partial \psi}{\partial z} \tag{17}$$

$$W = -\frac{1}{r}\frac{\partial \psi}{\partial r} \tag{18}$$

$$\Omega = \frac{1}{r}\frac{\partial^2 \psi}{\partial r^2} - \frac{1}{r^2}\frac{\partial \psi}{\partial r} + \frac{1}{r}\frac{\partial^2 \psi}{\partial z^2} \tag{19}$$

with

$$\mathrm{U} = \frac{\mathrm{u}^*\mathrm{R}}{\alpha} \tag{20}$$

$$\mathrm{W} = \frac{\mathrm{w}^*\mathrm{R}}{\alpha} \tag{21}$$

$$\Omega = \frac{\Omega^*\mathrm{R}^2}{\alpha} \tag{22}$$

$$\psi = \frac{\psi^*}{\mathrm{R}\,\alpha} \tag{23}$$

$$\theta = \frac{\mathrm{T}^* - \mathrm{T}_\mathrm{F}^*}{\mathrm{T}_\mathrm{C}^* - \mathrm{T}_\mathrm{F}^*} \tag{24}$$

$$\mathrm{S} = \frac{\mathrm{S}^* - \mathrm{S}_{\mathrm{sup}}^*}{\mathrm{S}_{\mathrm{inf}}^* - \mathrm{S}_{\mathrm{sup}}^*} \tag{25}$$

The following dimensionless numbers are introduced:

$$R_{T,nf} = \frac{\rho_0(1-\varphi)g\ \beta_T\,\Delta T R^3}{\mu_{nf}\alpha_{nf}} \tag{26}$$

$$Pr_{nf} = \frac{\upsilon_{nf}}{\alpha_{nf}} \tag{27}$$

$$Da = \frac{K}{R^2} \tag{28}$$

$$N = \frac{\beta_s \Delta S}{\beta_T \Delta\theta} \tag{29}$$

$$Le = \frac{\alpha}{D} \tag{30}$$

$$Du = \frac{N_{TC}\,\Delta S}{\alpha\,\Delta\theta} \tag{31}$$

$$Sr = \frac{N_{CT}\,\Delta\theta}{D\Delta S} \tag{32}$$

$$\bar{\Lambda} = \frac{\Lambda_{nf}}{\Lambda_e} \tag{33}$$

Non-dimensional boundary conditions

To the equations above, we add the boundary conditions in the following dimensionless form:

$$r = 0, \qquad \psi = 0, \left.\frac{\partial \theta}{\partial r}\right|_{r=0} = 0, \quad \left.\frac{\partial S}{\partial r}\right|_{r=0} = 0, \qquad \Omega|_{r=0} = 0 \tag{34}$$

$$r = 1, \psi = \frac{\partial \psi}{\partial r} = \frac{\partial \psi}{\partial z} = 0, \quad \left.\frac{\partial \theta}{\partial r}\right|_{r=1} = 0, \ \left.\frac{\partial S}{\partial r}\right|_{r=1} = 0, \quad \Omega|_{r=1} = \frac{2}{dr^2}\psi|_{r=1-\Delta r} \tag{35}$$

$$z = 0, \psi = \frac{\partial \psi}{\partial r} = \frac{\partial \psi}{\partial z} = 0, \qquad \theta = 1, \quad S = 1, \Omega|_{z=0} = \frac{1}{r}\frac{2}{dz^2}\psi|_{z=dz} \tag{36}$$

$$z = A, \psi = \frac{\partial \psi}{\partial r} = \frac{\partial \psi}{\partial z} = 0, \qquad \theta = 0, \quad S = 0, \qquad \Omega|_{z=A} = \frac{1}{r}\frac{2}{dz^2}\psi|_{z=A-dz} \tag{37}$$

Heat and mass transfer

The heat and mass transfer on the horizontal active wall is represented by the average of Nusselt number, Nu and average of Sherwood number, Sh respectively, defined by the following relations:

$$Nu = -2A\int_0^1 \left.\frac{\partial\theta}{\partial z}\right|_{z=0} dr \quad (38)$$

$$Sh = -2A\int_0^1 \left.\frac{\partial S}{\partial z}\right|_{z=0} dr \quad (39)$$

3. Resolution Process

The phenomenon of thermosolutal convection is governed by a system of nonlinear partial differential equations and has a very strong coupling, not admitting an analytical solution, so recourse to numerical methods is mandatory. We have opted for the use of the finite volume method [32,33] to discretize all the equations. The algebraic form of the equations obtained, to which we add boundary conditions, are solved using the double-scan method. The stream function equation is solved using the Simultaneous Over-Relaxation (SOR) method [34-36]. The convergence criterion is given by:

$$\frac{\sum_i\sum_j|\chi_{i,j}^{n+1}-\chi_{i,j}^{n}|}{\sum_i\sum_j|\chi_{i,j}^{n+1}|} \le 10^{-5} \quad (40)$$

Validation of results

To confirm the correct behavior of the numerical model, the grid convergence test is performed at different grid levels and by restricting $Ha = 0$, $N = 1$, $A = 2$ $Pr = 0.71$, $Le = 10$, $\varphi = 0.05$, $Da = 0.001$, $Sr = 1$ et $Du = 1$, $\left(1+\frac{1}{\beta}\right) \approx 1$ and are shown in Table 1. For this purpose, the average heat and mass fluxes are calculated. We see that at the grid sizes 151 × 151 and 161 × 161.

Table 1. Grid independency study

Size of the grid	Nu	Error %
121 × 121	2.52040109249	1.85×10^{-3}
131 × 131	2.56792843486	6.3×10^{-4}
141 × 141	2. 58442832678	3×10^{-6}
151 × 151	2.58452261179	3×10^{-6}
161 × 161	2.58461689682	

The results obtained are in perfect agreement with those of other authors who deal with the same problem [4]. By calculating the average Nusselt number with respect to the number of thermal Rayleigh number and by fixing $Ha = 0$, $N = 1$, $Pr = 0.71$, $Le = 10$, $\varphi = 0.05$, $Da = 0.001$, $Sr = 1$ et $Du = 1$, $\left(1+\frac{1}{\beta}\right) \approx 1$ because we gave β a large value as shown in Table 2. From the data (fig. 2), we validated the results obtained from the present study (fig. 3).

Table 2. Comparison of the numerical procedure with [4]

	Absolute variation of $Nu_{R_{T=10}}$ to $Nu_{R_T=10^4}$ [4]	**Relative variation of $Nu_{R_{T=10}}$ to $Nu_{R_{T=10^4}}$ [4]**	**Absolute variation of $Nu_{R_{T=10}}$ to $Nu_{R_T=10^4}$ (This study)**	**Relative variation of $Nu_{R_{T=10}}$ to $Nu_{R_{T=10^4}}$ (This study)**
A=1	2×10^{-2}	8×10^{-3}	$1{,}9 \times 10^{-2}$	$7{,}4 \times 10^{-3}$
A=2	$4{,}2 \times 10^{-2}$	$1{,}6 \times 10^{-2}$	4×10^{-2}	$1{,}5 \times 10^{-2}$
A=3	$6{,}4 \times 10^{-2}$	$2{,}5 \times 10^{-2}$	6×10^{-2}	$2{,}3 \times 10^{-2}$

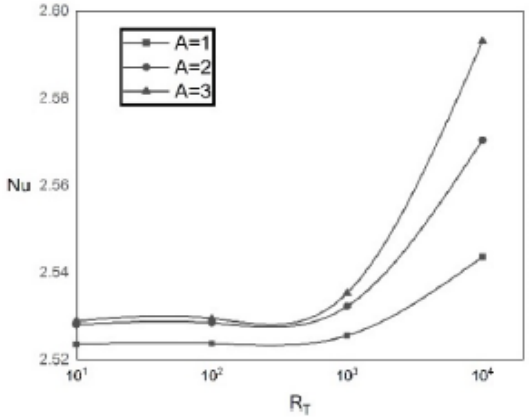

Fig. 2. Effect of R_T on Nu [4]

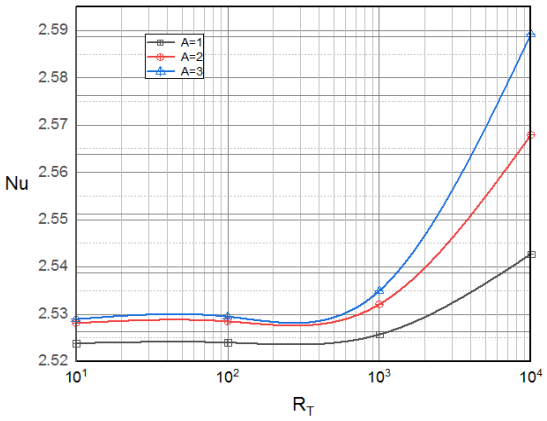

Fig. 3. Effect of of R_T on Nu (This study)

4. Results and Discussion

4.1. Effect of Casson's Fluid Parameter, β

Influences of Casson's fluid parameters on heat and mass transfer fig. (4) and Figs. (5) with $A = 3$, $R_{T,nf} = 10^4$, $N = 1$, $Pr_{nf} = 6.8$, $Le = 2.5$, $\varphi = 0.05$, $Da = 0.001$, $\bar{\Lambda} = 1$, $Sr = 1$ et $Du = 1$. Casson's fluid parameter β, varies from 0.1 to 1. We see in these figures, that the heat and mass transfer increases with the

increase of β. This increase results from the viscosity of the fluid which decreases as the quantity of Casson's parameter increases, and this reduction in viscosity leads to better thermosolutal transfer. we noticed that the rate of heat and mass transfer is high when β is between 0.1 and 0.4 compared to β between 0.4 and 1. On the other hand, an opposite behavior is observed in the heat and mass transfers with respect to the Hartmann number (Ha). This fact is proved by the production of resistive forces (Lorentz force) in the flow domain due to the improvement of Hartmann numbers as well as the reduction of the kinetic energy of particles.

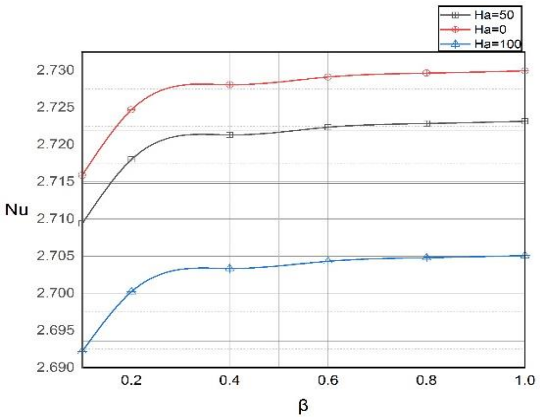

Fig. 4. Effect of β on Nu

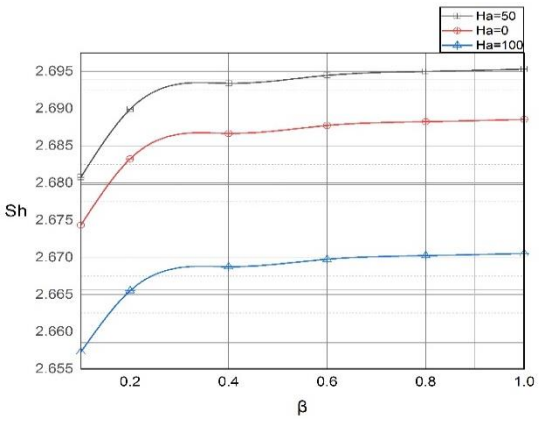

Fig. 5. Effect of β on Sh

4.2. Effect of the Thermal Conductivity Ratio, $\bar{\Lambda}$

Figures 6 and 7 show the influence of the ratio of thermal conductivities on the heat and mass transfer for $A = 3$, $R_{T,nf} = 10^4$, $N = 1$, $Pr_{nf} = 6.8$, $Le = 2.5$, $\varphi = 0.05$, $Da = 0.001$, $Sr = 1$, $Du = 1$ and $\bar{\Lambda}$ varying between 1 and 3, β between 0.1 and 1, Ha between 0 and 50. The average Nusselt number and average Sherwood number evolve in a monotonous way with the increase of the parameter of the ratio of the thermal conductivities. This increase results from the argument of thermal and solutal volume forces. it is noted on the same figures that the values of the average Nusselt number and average Sherwood number increase when the Casson parameter increases for the case Ha=0. Whereas a contrary behavior is observed that the values of average Nusselt number and average Sherwood number decrease with the increase of the Casson parameter for the case Ha=50. This decrease is due to the fact that the resistive forces are greater than the thermosolutal volume forces.

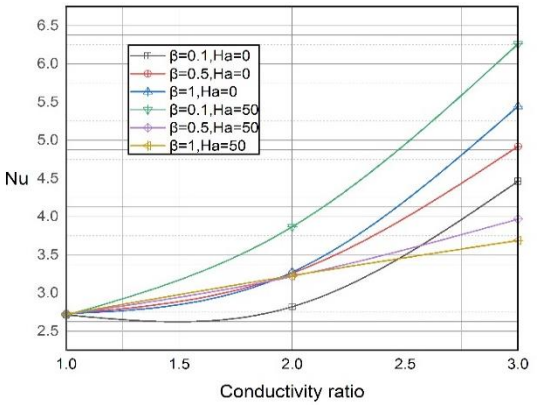

Fig. 6. Effect of $\bar{\Lambda}$ on Nu

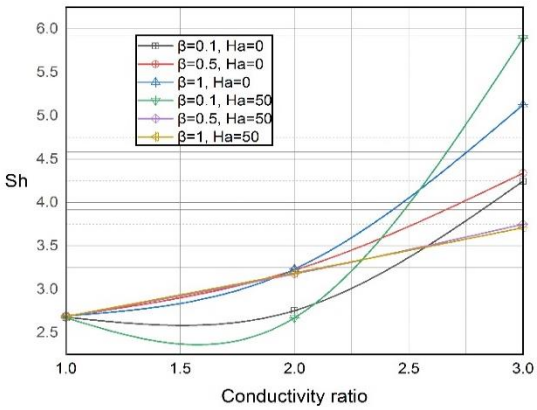

Fig. 7. Effect of $\bar{\Lambda}$ on Sh

4.3. Effect of Thermal RAYLEIGH Number, $R_{T,nf}$

Figures 8 and 9 show the effect of thermal Rayleigh number on heat and mass transfer respectively. Notes in Figures 8 and 9 show the average Nusselt number and average Sherwood number, which remain unchanged for $R_{T,nf} \leq 5 \times 10^2$ When the Thermal Rayleigh number exceeds the threshold $R_{T,nf} = 5 \times 10^2$. We see an increase in the average Nusselt number and average Sherwood number with the increase in $R_{T,nf}$, which results on the one hand from the increase in the thrust forces and the decrease in the viscous forces. due to the increase in $R_{T,nf}$. The elevation of the thrust forces causes an increase in the kinetic energy of the particles leading to a better thermosolutal transfer. On the

other hand, the decrease in viscous forces results in the viscosity of the fluid decreasing and this reduction in viscosity leads to better thermosolutal transfer. As the rate of buoyancy increases, the flow inside the enclosure will be driven by the mixed effect of thermal buoyancy and concentration forces which result in a marked increase in the mean value of Nusselt number and Sherwood number. We also noted that the effect of thermal Rayleigh number and Buoyancy ratio on heat and mass transformation increases with increasing geometric aspect ratio, A.

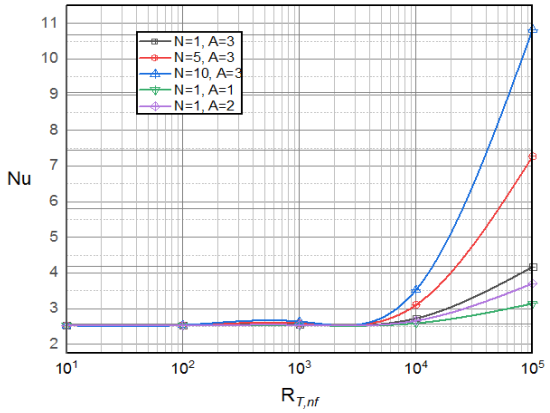

Fig. 8. Effect of $R_{T,nf}$ on Nu

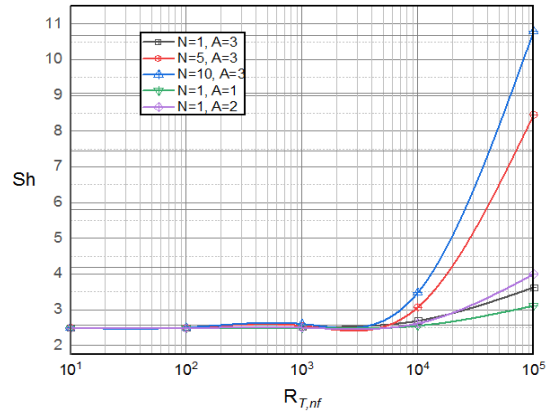

Fig. 9. Effect of $R_{T,nf}$ on Sh

4.4. *Effect of the Variation of SORET and DUFOUR Numbers*

From figure 10, we notice that the average Sherwood number is decreased with the increase of the Soret number evaluates between 0.1 and 1.2. On the one hand, the increase in the Soret coefficient, which describes the phenomenon of thermodiffusion, causes a decrease in mass transfer. On the other hand, the increase in Ha number decreases the mass transfer. This decrease results from the improvement of resistive force with increase of Ha. Therefore, this improvement of resistive force leads to a reduction of the kinetic energy of the particles.

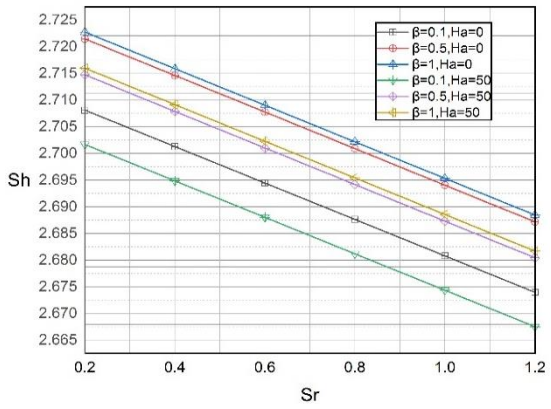

Fig. 10. Effect of Sr on Sh

In Figure 11, the Dufour effect on the heat transfer has been represented. it can be seen in this figure that the average Nusselt number value decreases with the increase in the Dufour number. The increase in Dufour number causes mass diffusion. The latter is responsible for reducing heat transfer. As for Casson's fluid parameter, it causes an increase in heat transfer.

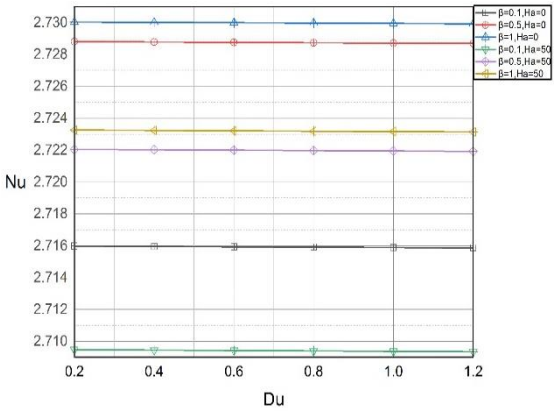

Fig. 11. Effect of Du on Nu

5. Conclusions

This study focused on the natural convection of thermosolutes in cylindrical cavities filled with a Casson nanofluid, leading to the following conclusions:

Heat and mass transfer increase with increasing Casson fluid parameter. This is explained by the importance of the intensity of the flow with the increase of the Casson fluid parameter; this increase is important for the case of β between 0.1 and 0.4. Conversely, Hartmann number (Ha), when it goes high, causes a decrease in heat and mass transfer. This decrease is greater for high values of the Hartmann number (Ha). Increase in Ha number causes resistive forces (the Lorentz force) in the flow domain as well as reduction in the kinetic energy of the particles. Heat and mass transfer increase with increasing number of thermal conductivities ratio. This increase results from the

argumentation of the forces of thermal and solutal volume. One notes that average Nusselt number and average Sherwood number increase when the Casson parameter increases for the case $Ha = 0$. When at the number Ha=50, the average Nusselt number and average Sherwood number are decreased with the increase in β. This decrease is due to the fact that the resistive forces are greater than the thermosolutal volume forces.

It can be seen that for $R_{T,nf} \leq 5 \times 10^2$, the average Nusselt number and the Sherwood number remain unchanged. When the thermal Rayleigh number exceeds this threshold $R_{T,nf} = 5 \times 10^2$, the heat transfer and mass increase. This increase results from increased kinetic energy of the particles due to enhanced thermal Rayleigh number. We notice that the average Sherwood number and average Nusselt number increase with an increase in the number of thrust ratios; this fact is proven by the production of the forces of thermal buoyancy and concentration, which lead to a clear increase in the average value of the Nusselt number and Sherwood number. We notice that the average Sherwood number and average Nusselt number decreased respectively with the increase of the number of Soret and number of Dufour because the two coefficients of Soret and Dufour create phenomenon of the thermodiffusion. Therefore, the increasing in this parameter is provoked respectively by a decrease in mass and heat transfer. This helps in many applications such as metallurgy, electrochemistry, biology, geophysics, chemical systems and processes.

Nomenclature

Symbol	Meaning	Unit
$\boldsymbol{A}$	Geometric aspect ratio $(\frac{L}{R})$	
$\boldsymbol{B}$	Magnetic field strength	$[T]$
$\boldsymbol{J}$	electrical current density	$[A/m^2]$
$\boldsymbol{E}$	electric field strength	[V/m]
$\boldsymbol{P}$	Pressure	[bar]
$\boldsymbol{S}^*$	Concentration	[Kg/m^3]
$\boldsymbol{S}$	Dimensionless concentration	
$\boldsymbol{C_F}$	Forchheimer coefficient	
$\boldsymbol{D}$	Mass diffusivity	$[m^2/\mathrm{s}]$
$\boldsymbol{Da}$	Darcy number	
$\boldsymbol{Du}$	Dufour number	
$\boldsymbol{Ha}$	Hartmann number	
$\boldsymbol{K}$	Permeability of the porous medium	$[m^2]$
$\boldsymbol{Le}$	Lewis number	
$\boldsymbol{L}$	Cylinder height	$[m]$
$\boldsymbol{R}$	Cylinder radius	$[m]$
$\boldsymbol{r}^*$	Radial coordinate	$[m]$
$\boldsymbol{r}$	Dimensionless radial coordinate	
$\boldsymbol{z}^*$	Axial coordinate	$[m]$
$\boldsymbol{z}$	Dimensionless axial coordinate	
$\boldsymbol{N}$	Buoyancy ratio	
$\mathbf{N_{CT}}$	Soret coefficient	[Kg /m. K. s]
$\mathbf{N_{TC}}$	Dufour coefficient	$[m^5.K/$ Kg. s]
$\boldsymbol{Nu}$	Average Nusselt number	
$\boldsymbol{Pr_{nf}}$	Prandtl number	
$\boldsymbol{R_{T,nf}}$	Thermal Rayleigh number	
$\boldsymbol{Sh}$	Average Sherwood Number	
$\boldsymbol{Sr}$	Soret number	
$\boldsymbol{T}^*$	Temperature	$[K]$
$\boldsymbol{\theta}$	Dimensionless temperature	
$\boldsymbol{U}^*$	Radial component of velocity	$[m/s]$
$\boldsymbol{U}$	Dimensionless radial component of velocity	
$\boldsymbol{W}^*$	Axial component of velocity	$[m/s]$
$\boldsymbol{W}$	Dimensionless axial component of velocity	
$\boldsymbol{\beta}$	Casson fluid parameter	
$\boldsymbol{\beta_T}$	Thermal expansion coefficient	$[K^{-1}]$
$\boldsymbol{\beta_s}$	Solute expansion coefficient	[Kg. mol/l]
$\boldsymbol{\rho_0}$	Reference density of the fluid	[Kg/m^3]
$\boldsymbol{\mu_{nf}}$	Dynamic viscosity of the nanofluid	[Kg/ m. s]
$\boldsymbol{\widetilde{\mu_{nf}}}$	Effective dynamic viscosity of the nanofluid	[N. s/m^2]
$\boldsymbol{\upsilon_{nf}}$	Kinematic viscosity of the nanofluid	[m^2/s]
$\boldsymbol{\varphi}$	Volume fraction of nanoparticles	
Ω^*	Component of the rotational vector of velocities	
Ω	Component of the dimensionless rotational velocity vector	
$\boldsymbol{\psi}^*$	stream function	
$\boldsymbol{\psi}$	Dimensionless stream function	
$\boldsymbol{\varepsilon}$	Porosity	
$\boldsymbol{\Lambda_{nf}}$	Thermal conductivity of the nanofluid	[W/m. K]
$\boldsymbol{\Lambda_e}$	Thermal conductivity of the porous medium,	[W/m. K]
$\boldsymbol{\overline{\Lambda}}$	Conductivity ratio	
$\boldsymbol{\alpha}$	Thermal diffusivity of the saturated porous medium	$[m^2/\mathrm{s}]$
$\boldsymbol{\alpha_{nf}}$	Thermal diffusivity of the nanofluid	$[m^2/\mathrm{s}]$
$\boldsymbol{\sigma_{nf}}$	Electrical conductivity of the nanofluid	$[A^2.s^3/$ m^3. Kg]

Conflicts of Interest

The author declares that there is no conflict of interest regarding the publication of this article.

References

[1] Animasaun, I.L., 2016. Double diffusive unsteady convective micropolar flow past a vertical porous plate moving through binary mixture using modified Boussinesq approximation. *Ain Shams Engineering Journal, 7(2)*, pp.755-765.

[2] El Hamma, M., Taibi, M., Rtibi, A., Gueraoui, K. and Bernatchou, M., 2022. Effect of magnetic field on thermosolutal convection in a cylindrical cavity filled with nanofluid, taking into account Soret and Dufour effects. *JP Journal of Heat and Mass Transfer, 26*, pp. 1-26. http://dx.doi.org/10.17654/0973576322009

[3] Chen, S., Yang, B., Luo, K.H., Xiong, X. and Zheng, C., 2016. Double diffusion natural convection in a square cavity filled with nanofluid. *International Journal of Heat and Mass Transfer, 95*, pp.1070-1083.

[4] El Hamma, M., Rtibi, A., Taibi, M., Gueraoui, K., Bernatchou, M., 2022. Theoretical and Numerical Study of Thermosolutal Convection in a Cylindrical Porous Cavity Filled with a Nanofluid and Taking into Account Soret and Dufour Effects. *International Journal on Engineering Applications (I.R.E.A.), 10*, (1) DOI: https://doi.org/10.15866/irea.v10i1.20809

[5] Hirpho, M. and Ibrahim, W., 2022. Modeling and simulation of hybrid Casson nanofluid mixed convection in a partly heated trapezoidal enclosure. *International Journal of Thermofluids, 15*, p. 100166. https://doi.org/10.1016/j.ijft.2022.100166

[6] Shah, I.A., Bilal, S., Noeiaghdam, S., Fernandez-Gamiz, U. and Shahzad, H., 2022. Thermosolutal natural convection energy transfer in magnetically influenced casson fluid flow in hexagonal enclosure with fillets. *Results in Engineering*, *15*, p.100584.

[7] Alwawi, F.A., Alkasasbeh, H.T., Rashad, A.M. and Idris, R., 2020. MHD natural convection of Sodium Alginate Casson nanofluid over a solid sphere. *Results in physics*, *16*, p.102818.

[8] Gbadeyan, J.A., Titiloye, E.O. and Adeosun, A.T., 2020. Effect of variable thermal conductivity and viscosity on Casson nanofluid flow with convective heating and velocity slip. *Heliyon*, *6*(1). https://doi.org/10.1016/j.heliyon.2019.e03076

[9] Haq, R.U., Nadeem, S., Khan, Z.H. and Okedayo, T.G., 2014. Convective heat transfer and MHD effects on Casson nanofluid flow over a shrinking sheet. *Central European Journal of Physics*, *12*, pp.862-871.

[10] Ibrahim, W. and Anbessa, T., 2020. Three-dimensional MHD mixed convection flow of Casson nanofluid with hall and ion slip effects. *Mathematical Problems in Engineering*, *2020*, pp.1-15.

[11] Kumar, K.G., Gireesha, B.J., Krishnamurthy, M.R. and Prasannakumara, B.C., 2018. Impact of convective condition on Marangoni convection flow and heat transfer in Casson nanofluid with uniform heat source sink. *Journal of Nanofluids*, *7*(1), pp.108-114.

[12] Nadeem, S., Haq, R.U. and Akbar, N.S., 2013. MHD three-dimensional boundary layer flow of Casson nanofluid past a linearly stretching sheet with convective boundary condition. *IEEE Transactions on Nanotechnology*, *13*(1), pp.109-115.

[13] Imtiaz, M., Hayat, T. and Alsaedi, A., 2016. Mixed convection flow of Casson nanofluid over a stretching cylinder with convective boundary conditions. *Advanced Powder Technology*, *27*(5), pp.2245-2256.

[14] Khan, M.I., Ahmad Khan, S., Hayat, T., Waqas, M. and Alsaedi, A., 2020. Modeling and numerical simulation for flow of hybrid nanofluid (SiO2/C3H8O2) and (MoS2/C3 H 8O2) with entropy optimization and variable viscosity. *International Journal of Numerical Methods for Heat & Fluid Flow*, *22*(8), pp.3939-3955. DOI 10.1108/HFF-10-2019-0756

[15] Alsabery, A.I., Chamkha, A.J., Saleh, H. and Hashim, I., 2017. Natural convection flow of a nanofluid in an inclined square enclosure partially filled with a porous medium. *Scientific reports*, *7*(1), p.2357.

[16] Khan, S.A., Hayat, T., Alsaedi, A. and Ahmad, B., 2021. Melting heat transportation in radiative flow of nanomaterials with irreversibility analysis. *Renewable and Sustainable Energy Reviews*, *140*, p.110739. https://doi.org/10.1016/j.rser.2021.110739.

[17] Sheremet, M.A., Pop, I. and Ishak, A., 2015. Double-diffusive mixed convection in a porous open cavity filled with a nanofluid using Buongiorno's model. *Transport in Porous Media*, *109*(1), pp.131-145.

[18] Hayat, T., Khan, S.A., Alsaedi, A. and Fardoun, H.M., 2020. Heat transportation in electro-magnetohydrodynamic flow of Darcy-Forchheimer viscous fluid with irreversibility analysis. *Physica Scripta*, *95*(10), p.105214. DOI 10.1088/1402-4896/abb7aa

[19] Miroshnichenko, I.V., Sheremet, M.A., Oztop, H.F. and Al-Salem, K., 2016. MHD natural convection in a partially open trapezoidal

cavity filled with a nanofluid. *International Journal of Mechanical Sciences*, *119*, pp.294-302. http://dx.doi.org/10.1016/j.ijmecsci.2016.11.001

[20] Khan, S.A., Hayat, T. and Alsaedi, A., 2022. Simultaneous features of Soret and Dufour in entropy optimized flow of Reiner-Rivlin fluid considering thermal radiation. *International Communications in Heat and Mass Transfer*, *137*, p.106297. https://doi.org/10.1016/j.icheatmasstransfer.2022.106297

[21] Basak, T., Roy, S., Matta, A. and Pop, I., 2010. Analysis of heatlines for natural convection within porous trapezoidal enclosures: effect of uniform and non-uniform heating of bottom wall. *International Journal of Heat and Mass Transfer*, *53*(25-26), pp. 5947-5961.

[22] Kairi, R.R., Roy, S. and Raut, S., 2023. Stratified thermosolutal Marangoni bioconvective flow of gyrotactic microorganisms in Williamson nanofluid. *European Journal of Mechanics-B/Fluids*, *97*, pp.40-52. https://doi.org/10.1016/j.euromechflu.2022.09.004

[23] Kairi, R.R., Shaw, S., Roy, S. and Raut, S., 2021. Thermosolutal marangoni impact on bioconvection in suspension of gyrotactic microorganisms over an inclined stretching sheet. *Journal of Heat Transfer, 143(3)*, p.031201. https://doi.org/10.1115/1.4048946

[24] Bernatchou, M., Gueraoui, K., Cherraj, M., Rtibi, A. and El Hamma, M., 2022, May. Analysis of the Magnetic Field Effect on Thermosolutal Convection Heat and Mass Transfer in a Square Cavity Filled with Nanofluid. In *International Conference on Integrated Design and Production* (pp. 605-615). Cham: Springer International Publishing.. https://doi.org/10.1007/978-3-031-23615-0_61

[25] Magagula, V.M., Shaw, S. and Kairi, R.R., 2020. Double dispersed bioconvective Casson nanofluid fluid flow over a nonlinear convective stretching sheet in suspension of gyrotactic microorganism. *Heat Transfer*, *49*(5), pp. 2449-2471. https://doi.org/10.1002/htj.21730

[26] Bilal, S., Shah, I.A., Marzougui, S. and Ali, F., 2023. Entropy analysis in single phase nanofluid in square enclosure under effectiveness of inclined magnetic field by executing finite element simulations. *Geoenergy Science and Engineering*, *225*, p.211483. https://doi.org/10.1016/j.geoen.2023.211483

[27] Shah, I.A., Bilal, S., Asjad, M.I. and Tag-ElDin, E.M., 2022. Convective heat and mass transport in Casson fluid flow in curved corrugated cavity with inclined magnetic field. *Micromachines*, *13*(10), p.1624. https://doi.org/10.3390/ mi13101624

[28] Bilal, S., Shah, I.A., Ghachem, K., Aydi, A. and Kolsi, L., 2023. Heat Transfer Enhancement of MHD Natural Convection in a Star-Shaped Enclosure, Using Heated Baffle and MWCNT–Water Nanofluid. *Mathematics*, *11*(8), p.1849. https://doi.org/10.3390/ math11081849.

[29] Zare Ghadi, A., Haghighi Asl, A., Valipour, M. S., 2014. Numerical modelling of double-diffusive natural convection within an arc shaped enclosure filled with a porous medium, *Journal of Heat and Mass Transfer Research*, *1(2)*, pp. 83-91. Doi: 10.22075/JHMTR.2014.183

[30] Lare, A.I., 2015. Casson fluid flow with variable viscosity and thermal conductivity along exponentially stretching sheet embedded in a thermally stratified medium with exponentially heat generation. *Journal of Heat and Mass Transfer Research*, *2*(2), pp.63-78. Doi: 10.22075/JHMTR.2015.346

[31] Ghaffarpasand, O., 2018. Characterization of unsteady double-diffusive mixed convection flow with soret and dufour effects in a square enclosure with top moving lid. *Journal of Heat and Mass Transfer Research*, *5*(1), pp.51-68. 10.22075/JHMTR.2017.880.1062

[32] Patankar, S.V., 1980. Numerical heat transfert and fluid flow. *Hemisphere*, New York.

[33] Bounouar, A., Gueraoui, K., Taibi, M., Lahlou, A., Driouich, M., Sammouda, M., Men-La-Yakhaf, S. and Belcadi, M., 2016. Numerical and mathematical modeling of unsteady heat transfer within a spherical cavity: Applications laser in medicine. *Contemporary Engineering Sciences*, *9*, pp.1183-1199.

[34] Mrabti, A., 1999. *Simulation Numérique d'Ecoulement de Convection Naturelle dans une Géométrie Cylindrique à Axe Verticale Soumise à l'Effet d'un Champ Magnétique ou d'un Gradient de Concentration* (Doctoral dissertation, Thèse, Faculté des Science Rabat).

[35] Sammouda, M., 2012. Modélisation théorique et numérique du phénomène de la convection naturelle et thermosolutale dans les milieux poreux à porosité variable. Thèse de Doctorat, Université Mohamed V, Morocco.

[36] Frankel, S.P., 1950. Convergence rates of iterative treatments of partial differential equations. *Mathematics of Computation, 4(30)*, pp.65-75.